Journal of Research in Pharmacy

Research Article

www.jrespharm.com

Antibacterial activity and cytocompatibility evaluation of cefpodoxime proxetil loaded eudragit rs 100 nanoparticles

Irfan AKARTAS [1] *, Aysegul ATES [2], Rengin REIS [3]

[1] State Laboratory, Ministry of Health, Turkish Republic of Northern Cyprus, TR-10, Mersin, Turkey.
[2] Department of Pharmaceutical Microbiology, Faculty of Pharmacy, Ege University, Izmir, Turkey.
[3] Department of Pharmaceutical Toxicology, Faculty of Pharmacy, Acıbadem Mehmet Ali Aydınlar University, Atasehir, Istanbul, Turkey.
* Corresponding Author. E-mail: iakartas@eul.edu.tr (I.A.); Tel. +90-392-225 30 75, Fax. +90-392-225 36 86.

Received: 10 Jun 2023 / Revised: 03 Jul 2023 / Accepted: 04 Jul 2023

ABSTRACT: The main purpose of this study is to design Cefpodoxime proxetil (CFP) loaded Eudragit RS 100 (ERS) nanoparticles to provide prolonged drug release, the enhanced oral efficacy of the drug at a lower oral dose. CFP-loaded nanoparticles are prepared by the single-emulsion solvent evaporation method with different drug:polymer ratios, F1 (CFP:ERS=1:1) and F2 (CFP:ERS=1:2). Physicochemical characterization, antibacterial activity, cytotoxicity profiles of nanoparticles are examined. F1 and F2 nanoparticles have a particle size of 236.70±3.05 and 258.87±11.32 nm, spherical shape, and a porous surface under SEM. The zeta potential values of F1 and F2 nanoparticles were 22.13±1.01 and 25.80±2.01 mV, and the encapsulation efficiencies were 34.37±3.71% and 55.78±3.52%, respectively. Since F2 nanoparticles have a smaller particle size, higher zeta potential, and encapsulation efficiency, this formulation was chosen as superior, and the subsequent experiments were continued with this formulation. The antibacterial activity of F2 nanoparticles against *E.coli* was found to be 2 times more effective than CFP. Cytotoxicity studies revealed that the cell viabilities in BEAS-2B and HepG2 cells were higher with the exposure to CFP nanoparticles (200 µg/ml) compared to CFP (100 µg/ml) alone. CFP nanoparticles have excellent efficacy and a cytocompatible profile in inhibiting the growth of bacteria compared to free CFP.

KEYWORDS: Cefpodoxime; eudragit; nanoparticles; oral application; antibacterial; time kill; cytotoxicity.

1. INTRODUCTION

Oral administration has been a convenient route of drug delivery in recent years. Due to enhanced patient compliance, flexible dosing, and fewer requirement on health professionals and hospital visits, oral formulations are advantageous when compared with the intravenous route. Despite all these advantages, the acidic pH of the gastrointestinal tract, digestive enzymes, mucosal barrier, and gastrointestinal side effects limit the oral administration of drugs [1,2]. In order to overcome these obstacles, nanoencapsulation technology has been used to produce nano-based drug delivery systems.

Polymeric nanoparticles are colloidal systems with a diameter of 1-1000 nm. It consists of active pharmaceutical ingredients entrapped in macromolecular substances such as polymers. Nanoparticles have abilities such as drug transport, controlled release at the target site, large volume-to-surface ratio, high stability, and non-immunogenicity. In addition to all these advantages, it is superior to conventional oral and intravenous administration routes in terms of effectiveness [3]. Using different polymers to form nanoparticles provides better design by modifying physicochemical properties such as particle size, zeta potential, the solubility of the drug, and release properties (controlled or sustained release) [1]. Various types of polymers including temperature-, pH-, and redox-sensitive polymers can be used for the entrapment of active substances according to their chemical or physical properties [4]. In order to provide the stability of the drug in the acidic condition of the gastrointestinal tract, acid stable-pH sensitive polymers can be used such as Eudragit (polymethacrylate) [2].

Eudragit RS 100 (ERS), a poly(ethyl acrylate, methyl-methacrylate, and chlorotrimethyl-ammoniumethylmethacrylate) copolymer containing 4.5-6.8% quaternary ammonium groups, is used for the preparation of controlled-release drug delivery systems [5,6]. It is a cationic polymer, insoluble in water at

How to cite this article: Akartas I, Ates A, Reis R. Antibacterial activity and cytocompatibility evaluation of cefpodoxime proxetil loaded eudragit rs 100 nanoparticles. J Res Pharm. 2024; 28(2): 409-428.

ISSN: 2630-6344

http://dx.doi.org/10.29228/jrp.706

physiological pH but capable of swelling in the aqueous medium [7]. ERS is an advantageous polymer due to its high stability, suitable size distribution, and non-toxic feature [8]. ERS nanoparticles have the potential to encapsulate and increase the solubility and efficacy of poorly water-soluble drugs [9].

Although significant progress has been made in the development of antibiotics in recent years, there are difficulties in the treatment of intracellular infections. This difficulty arises from the inability of antibiotics to transport and act into cells, causing toxicity in healthy tissues and resistance of microorganisms to the drug [10]. Cefpodoxime proxetil (CFP) is a prodrug, third-generation cephalosporin with a broad spectrum of antibacterial activity. CFP is effective against many common gram-positive and gram-negative microorganisms and is used for the treatment of respiratory and urinary tract infections, gonorrhea, and skin or soft tissue infections. CFP is used in doses of 200-400 mg/day in respiratory and urinary tract infections, and 400-800 mg/day in skin infections. [11,12]. CFP is an orally administered and well-tolerated drug, however, it has only 50% oral bioavailability. In addition, CFP causes gastrointestinal side effects, commonly diarrhea, abdominal pain, nausea, vomiting, and rare adverse events including hemolytic anemia and agranulocytosis [12,13]. In order to overcome these obstacles and increase the efficacy of drugs, the development of nanoparticles is an innovative approach, in which researchers have shown great promise. Nanoparticles are an innovative approach with great promise in overcoming these side effects and increasing the effectiveness of drugs. In addition, the development of nanoparticle form by encapsulating antibacterial drugs into polymers can prevent biofilm formation, which plays an essential role in the development of drug resistance in microorganisms [14].

Many methods can be used to prepare nanoparticles including solvent evaporation, emulsification, nanoprecipitation, ionic gelation, and polymerization. In this study, the solvent evaporation method was used to prepare the nanoparticles. In this method, an oil-in-water emulsion is required to initialize nanoparticle production [15,16]. The solvent evaporation method is advantageous in that it can be applied to heat-sensitive drugs and to obtain nanoparticles with a small size (100 nm) and a narrow particle size distribution [17].

The main aim of this study is to develop CFP-loaded ERS nanoparticles, to enable the use of CFP at a lower oral dose, to provide long-term drug release, to reduce side effects, toxicity, and to reach higher antibacterial activity. With a detailed literature review, it was observed that antibacterial activity was not examined and the cytotoxicity profile was not elucidated in CFP-loaded ERS nanoparticles. Hence, developing CFP-loaded nanoparticles with a potent antibacterial activity and non-toxicity profile might be innovative and contribute to the literature for further studies. Looking at the literature history, developing CFP-loaded nanoparticles could be innovative in having a strong antibacterial activity and non-toxic profile and could contribute to the literature for further studies. For this purpose, the nanoparticles were developed and their physicochemical properties were characterized. *In vitro* release studies were performed and the release properties of drug-loaded nanoparticles and free drugs were compared. The antibacterial and time-kill activity of the formulations was tested, and the cytotoxicity profile of nanoparticles was evaluated in BEAS-2B human bronchial epithelial cells and HepG2 human liver hepatocellular carcinoma cells. Upon reviewing the literature, we realized that we had conducted the first study examining the time-kill activity of cefpodoxime. In light of the current study, it is predicted that CFP-loaded ERS nanoparticles can be an innovative and promising approach to oral therapy.

2. RESULTS

2.1. Particle size, polydispersity index (PDI), zeta potential measurement, and entrapment efficiency (EE%) of nanoparticles

F0, F1, and F2 were successfully prepared by the single emulsion solvent evaporation method and the number of components for each nanoparticle was presented in Table 1. Two different drug-loaded nanoparticles (F1 and F2) were prepared by keeping the amount of polymer constant and changing the amount of CFP. Blank nanoparticles were prepared for comparison with drug-loaded nanoparticles for further studies. The smaller-sized nanoparticles have a higher contact surface area. This increases cellular uptake and bioavailability by providing greater adhesion to the intestine [2,18]. In addition, due to their small size, nanoparticles can improve the pharmacokinetics, pharmacodynamics, and biodistribution of drugs and increase the efficacy of poorly water-soluble drugs [19,20]. Particle size, PDI, zeta potential, and EE% results of nanoparticles were demonstrated in Table 2. The mean particle size of F1 and F2 was determined as 236.70±3.05 and 258.87±11.32 respectively while F0 was 203.03±16.17 nm. PDI values of formulations were found in the range of 0.25-0.35. As a result of statistical studies, no significant difference was observed between the PDI values of F1 and F2 ($p>0.05$). While the zeta potential of the blank nanoparticles was measured as

19.47±0.61 mV, these values were measured as 22.13±1.01 and 25.80±2.01 mV respectively in the drug-loaded carriers F1 and F2. There is no statistically significant difference between the zeta potential values of F1 and F2 ($p>0.05$). The EE% of F1 and F2 were determined as 34.37±3.71 and 55.78±3.52% respectively.

Table 1: Components of ERS nanoparticles

Code	ERS (mg)	Acetone (mL)	CFP (mg)	Aqueous Phase
F0	100	6	-	20 mL 1% PVA
F1	100	6	100	20 mL 1% PVA
F2	100	6	50	20 mL 1% PVA

F0: Blank nanoparticles, F1: Cefpodoxime nanoparticles 1:1 (drug: polymer), F2: Cefpodoxime nanoparticles 1:2 (drug: polymer), ERS: Eudragit RS 100, CFP: Cefpodoxime proxetil, PVA: Poly(vinyl alcohol)

Table 2: Particle size, PDI, zeta potential, and EE% results of nanoparticles

Sample	Particle Size±SD (nm)	PDI±SD	Zeta Potential±SD (mV)	EE±SD (%)
F0	203.03±16.17	0.35±0.01	19.47±0.61	-
F1	236.70±3.05	0.25±0.03	22.13±1.01	34.37±3.71
F2	258.87±11.32	0.33±0.04	25.80±2.01	55.78±3.52

SD: Standard deviation

2.2. Morphological analysis of nanoparticles

Morphological analysis of CFP and CFP nanoparticles were examined by SEM. SEM is an excellent method to characterize the size, shape, and surface properties of produced nanoparticles due to quick and simple image acquisition [21]. SEM images of CFP and F2 were shown in Figure 1A and 1B. CFP particles appear to be different-sized and heterogenous prismatic crystals. The particle sizes range from 499.5 to 857 nm in diameter. F2 has a distinct spherical shape and porous surface with a narrow particle size distribution of 125.8-263.1 nm, a fact that is in similarity to the measurements of PCS.

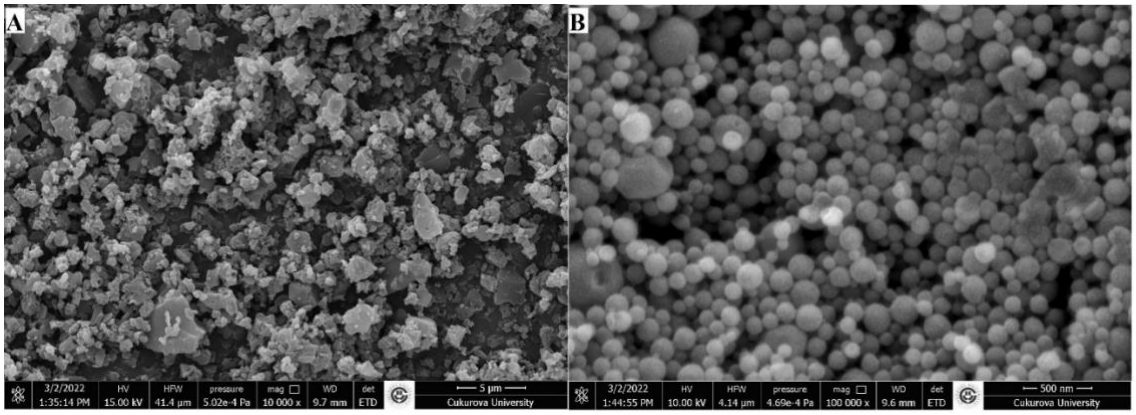

Figure 1: SEM images of CFP **(A)** and F2 **(B)**

2.3. Differential scanning calorimetry (DSC) analysis

DSC analysis was performed to investigate the thermal behavior of formulations and the interactions between the drug and polymer [22,23]. DSC thermograms of CFP, ERS, F0, and F2 were depicted in Figure 2. At the mentioned scanning rate (10°C/min), the thermogram of CFP exhibited a sharp endothermic peak at 96°C which indicates the melting transition temperature. The endothermic peak at 68°C in the thermogram of ERS was due to its glass transition temperature (Tg). In the DSC curves of F0 and F2, a broad endothermic peak was observed at 77°C indicating the Tg in common.

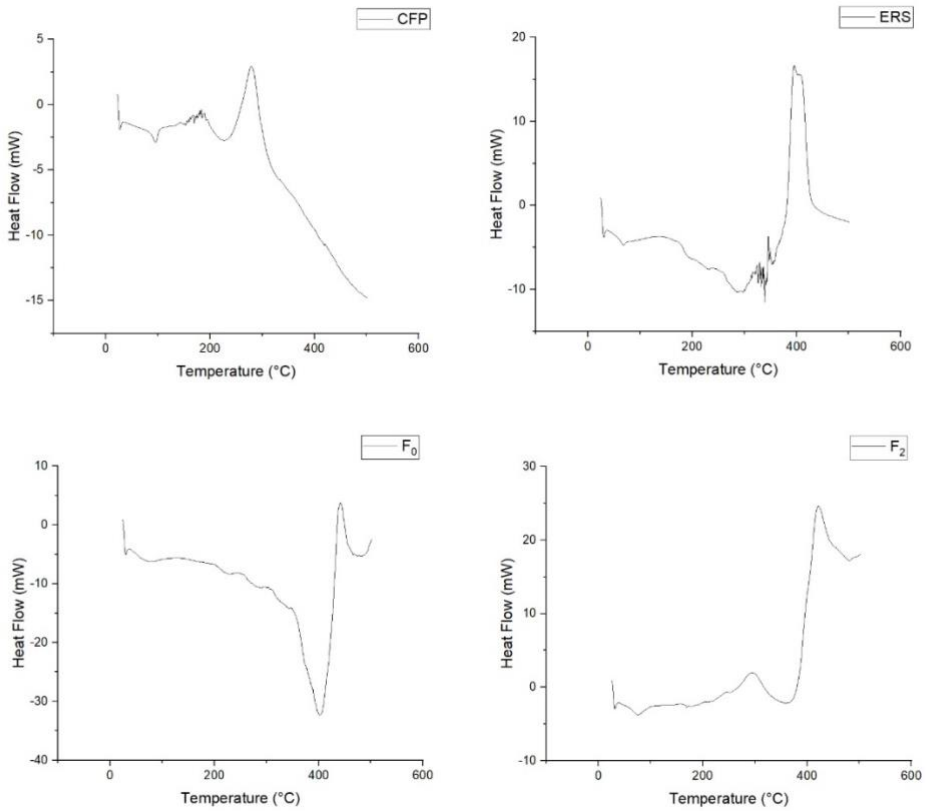

Figure 2: DSC thermograms of CFP, ERS, F0 and F2

2.4. X-ray diffraction (XRD) analysis

XRD analysis was performed to examine the crystalline or amorphous structure of drug and nanoparticle formulations [24]. The XRD patterns of CFP, F0, and F2 were presented in Figure 3. A hump peak for CFP was observed at 21.2°. A broad peak at 13.6 and an undistinct peak at 31.5 were detected in the XRD pattern of F0, which also characteristically appeared in ERS [25]. The XRD pattern of F2 is similar to that of F0. As a difference, the intensity of the broad peak observed at 13.6 in the pattern of F2 decreased in F0. In addition, the hump peak observed at 21.2 in the XRD pattern of CFP disappeared in the pattern of F2.

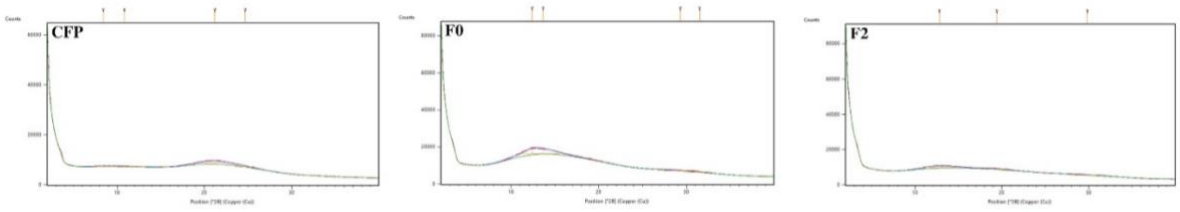

Figure 3: XRD patterns of CFP, F0, and F2

2.5. Fourier transform infrared (FT-IR) spectroscopy

FT-IR analyses were conducted in order to identify the chemical components of the formulation and determine the interactions between the drug and polymer [26,27]. Figure 4 presents the FT-IR spectra of CFP, ERS, F0, and F2. The characteristic peaks observed in CFP were 2935 (C-H), 3319 (N-H), 1531 (CN), and 1755 (C=O) stretching in β-lactam, 1271 (C-N=C) asymmetric stretching, and 1373 cm^{-1} (C-H) bending. In ERS, 2951(C-H) aliphatic stretching, 1720 (C=O) stretching, and 1234 cm^{-1} (C-O) stretching peaks appeared.

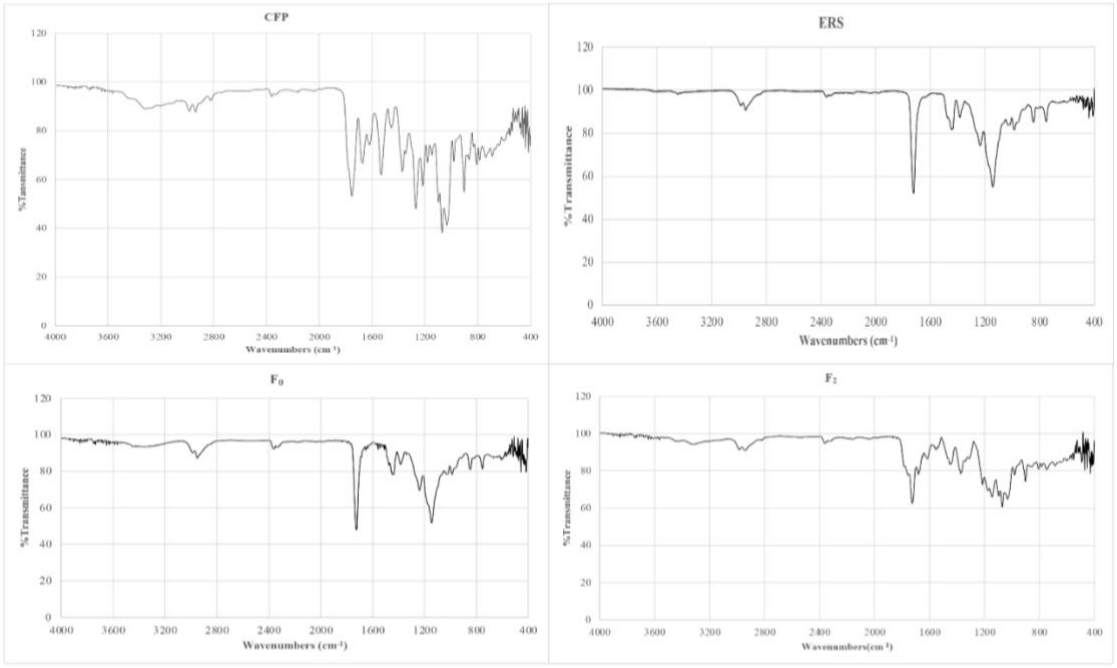

Figure 4: FT-IR spectra of CFP, ERS, F0, and F2

2.6. Proton nuclear magnetic resonance (^{1}H-NMR) spectroscopy

The physicochemical properties of nanoparticles and the molecular interactions between drug and polymer can be evaluated by NMR analysis [28]. ^{1}H-NMR spectrum of CFP, F0, and F2 was illustrated in Figure 5. The principle ^{1}H-NMR peak values of CFP and their appearance were presented in Table 3 and Figure 6 respectively. The characteristic signals of ERS polymer were observed in the spectra of F0. Similar spectra were obtained for F0 and F2, where the presence of principle CFP peaks was determined in the ^{1}H-NMR spectrum of F2.

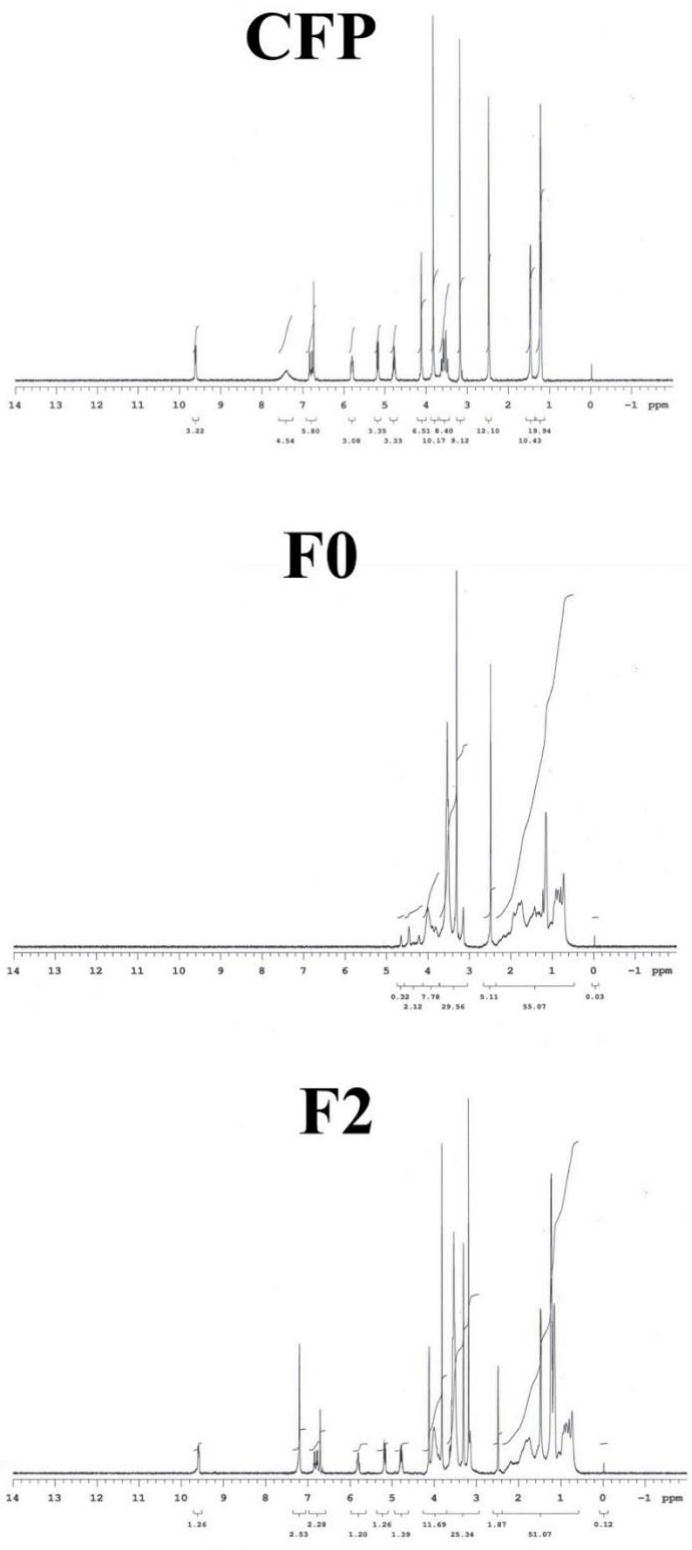

Figure 5: [1]H-NMR spectrum of CFP, F0, and F2

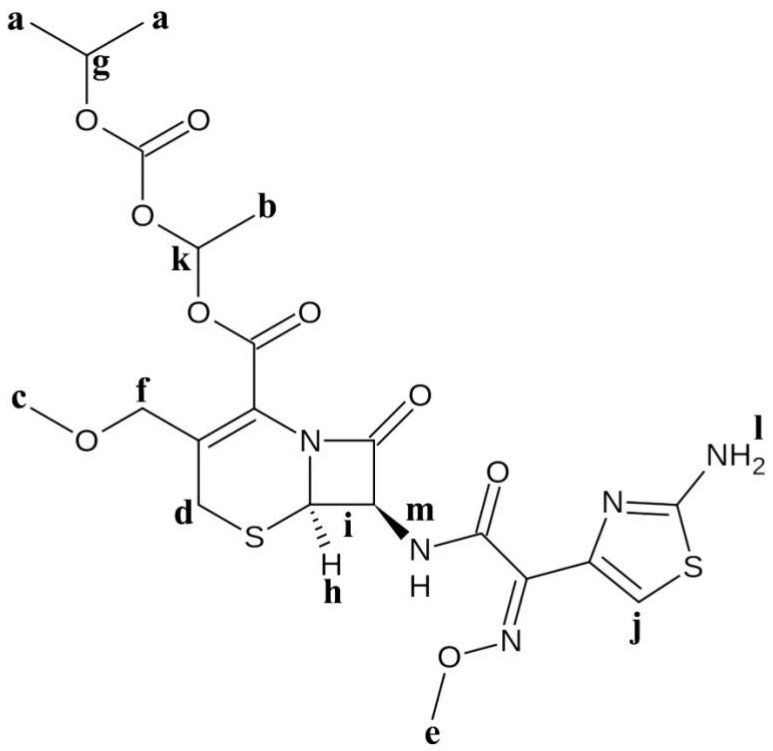

Figure 6: Chemical shift (δ) of hydrogens of cefpodoxime proxetil sorted alphabetically according to their appearance in ^{1}H-NMR

Table 3: Chemical structure and principle ^{1}H-NMR peak values of CFP

Position	Chemical shifts of CFP (ppm)
a	1.21-1.23 (m, 6H)
b	1.45-1.47 (m, 3H)
c	3.18 (s, 3H)
d	3.57-3.63 (m, 2H)
e	3.83 (s, 3H)
f	4.11 (s, 2H)
g	4.74-4.81 (m, 1H)
h	5.15-5.19 (m, 1H)
i	5.77-5.83 (m, 1H)
j	6.73-6.76 (s, 1H)
k	6.78-6.85 (m, 1H)
l	7.39 (s, br, 2H)
m	9.59-9.62 (m, 1H)

2.7. *In vitro* drug release profile and release kinetics

The *in vitro* release profile estimates in vivo absorption of a drug formulation. It plays an important role in the stability and quality control of drugs [29]. In the *in vitro* release study, at the end of the first 2 hours, the pH 1.2 medium was replaced with a pH 7.4 medium to simulate the gastrointestinal medium. The *in vitro* release profiles of CFP, F1, and F2 are shown in Figure 7. As can be clearly seen in the graph, the release rate of CFP from the nanoparticle is much slower than that of free CFP. 93.31±0.75% of CFP was released in the

first 3 hours. The release of CFP from F1 and F2 was 76.21±1.20 and 37.32±1.25% at the end of the 3rd hour respectively. The cumulative release values observed from CFP, F1, and F2 were 100.04±0.32, 88.67±1.30, and 86.20±1.11% at the end of 24 hours respectively.

Besides the 24-hour *in vitro* release study, the 2-hour release profile of CFP and nanoparticles in the gastrointestinal environment were compared in Figure 7.

In order to analyze the drug release mechanism from a drug delivery system, mathematical parameters were used. Fitting the *in vitro* drug release profiles to mathematical models which describe the drug release as a function of time gives significant data about the dissolution behavior of dosage forms [30]. The *in vitro* drug release data were fitted to many kinetic models including zero-order, first-order, Higuchi, Hixson-Crowell, Hopfenberg, Peppas-Sahlin, and Korsmeyer-Peppas using the DDSolver program. The coefficient of determination (R^2), adjusted coefficient of determination ($R^2_{adjusted}$), Akaike Information Criterion (AIC), and Model Selection Criterion (MSC) were selected as the most common criteria for evaluating kinetic models. The release kinetic values were summarized in Table 4. The model with the highest R^2, $R^2_{adjusted}$, MSC, and lowest AIC was selected as the best model [31]. The release profile of CFP fitted best to the Hopfenberg model. This model shows the diffusion and relaxation behavior of permeability [32]. Korsmeyer-Peppas was the best-fitted kinetic model for both F1 and F2.

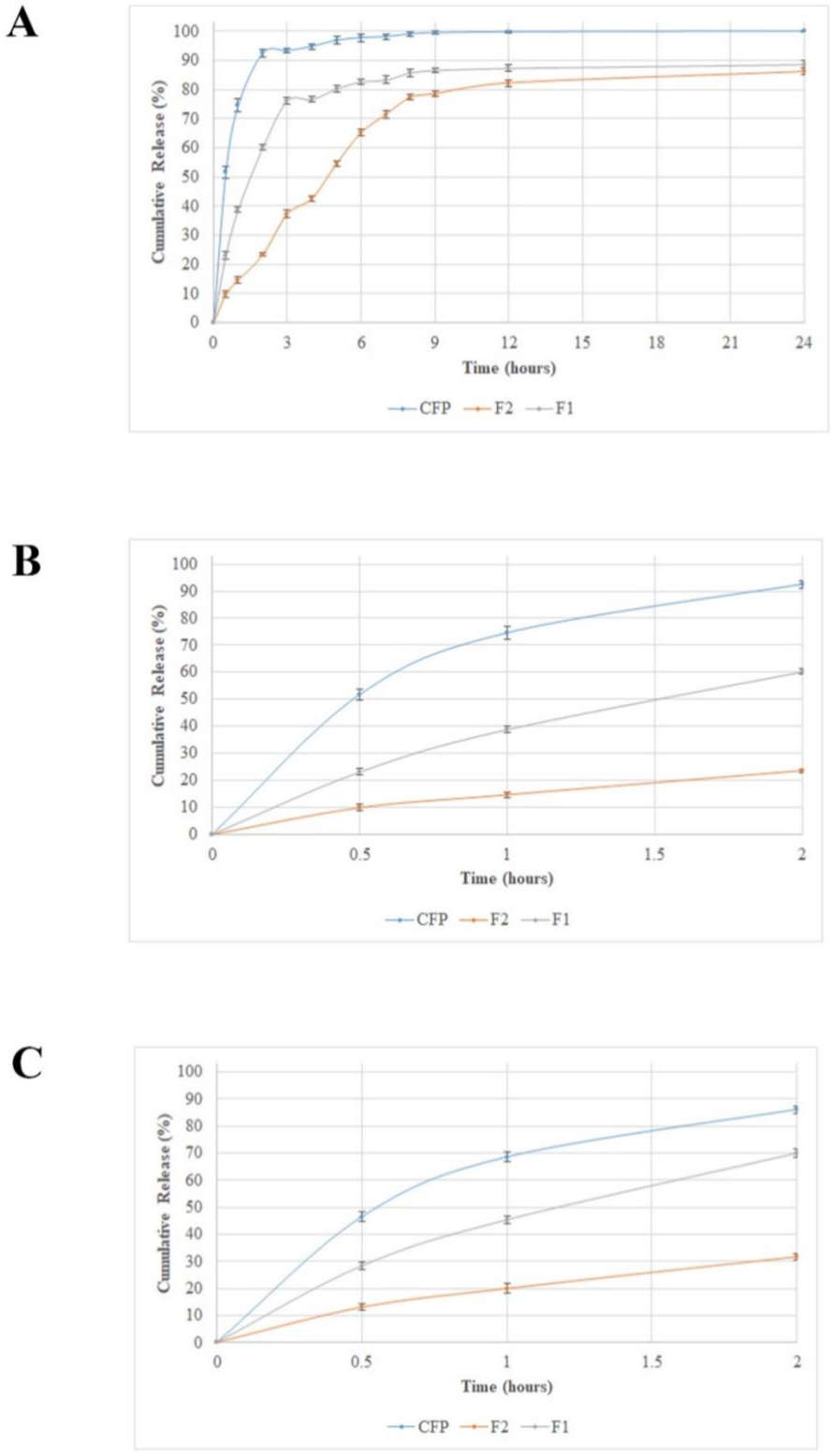

Figure 7: *In vitro* release profiles of CFP, F1, and F2. **A)** first 2 hours pH 1.2 HCl, next 22 hours pH 7.4 PBS medium. **B)** pH 1.2 HCl medium for 2 hours. **C)** pH 7.4 PBS medium for 2 hours.

Table 4: *In vitro* release kinetic models for CFP, F1, and F2.

Formulation	Kinetic Model	R^2	$R^2_{adjusted}$	AIC	MSC
CFP	Zero-order	-2.930	-2.930	139.516	-2.776
F1		-1.208	-1.208	131.718	-1.560
F2		0.250	0.250	119.152	-0.120
CFP	First order	0.993	0.993	57.598	3.526
F1		0.917	0.917	89.150	1.715
F2		0.977	0.977	73.708	3.375
CFP	Higuchi	-0.175	-0.175	123.823	-1.569
F1		0.504	0.504	112.299	-0.066
F2		0.876	0.876	95.722	1.682
CFP	Hixson-Crowell	-0.284	-0.284	124.969	-1.657
F1		0.638	0.638	108.225	0.247
F2		0.971	0.971	77.000	3.122
CFP	Hopfenberg	0.993	0.992	59.604	3.371
F1		0.916	0.909	91.154	1.561
F2		0.977	0.975	75.712	3.221
CFP	Peppas-Sahlin	0.977	0.972	76.698	2.057
F1		0.971	0.966	79.289	2.473
F2		0.989	0.986	68.613	3.767
CFP	Korsmeyer-Peppas	0.932	0.926	88.715	1.132
F1		0.999	0.999	5.218	5.605
F2		0.993	0.992	23.348	4.057

2.8. Antibacterial activity test

MIC values were defined after 24 hours of incubation. When the document published by EUCAST for quality control strains was examined, it was determined that the MIC range of CFP for *E.coli* ATCC 25922 was given as 0.25-1 µg/mL. In this study, the antibacterial activity of nanoparticles and CFP was evaluated, and MIC values of CFP, F2, and F0 for *E.coli* ATCC 25922 are summarized in Table 5. In light of antibacterial activity results, it was found that the MIC value of F2 was 2 times lower than the MIC value of CFP. The MIC value of F0 was evaluated as 2048 µg/mL.

Table 5: MIC values of formulations against *E.coli ATCC 25922*

Formulations	MIC Values (µg/ml)
CFP	1
F2	0.5
F0	2048

2.9. Time-kill assay

The time-kill curve of CFP, F2, F0, and growth control is shown in Figure 8. When the time-kill results were examined, it was determined that the efficiency of CFP decreased after the 4th hour and that its activity clearly decreased after the 6th hour. Since the activity of F0 is almost absent, similar results were obtained with growth control.

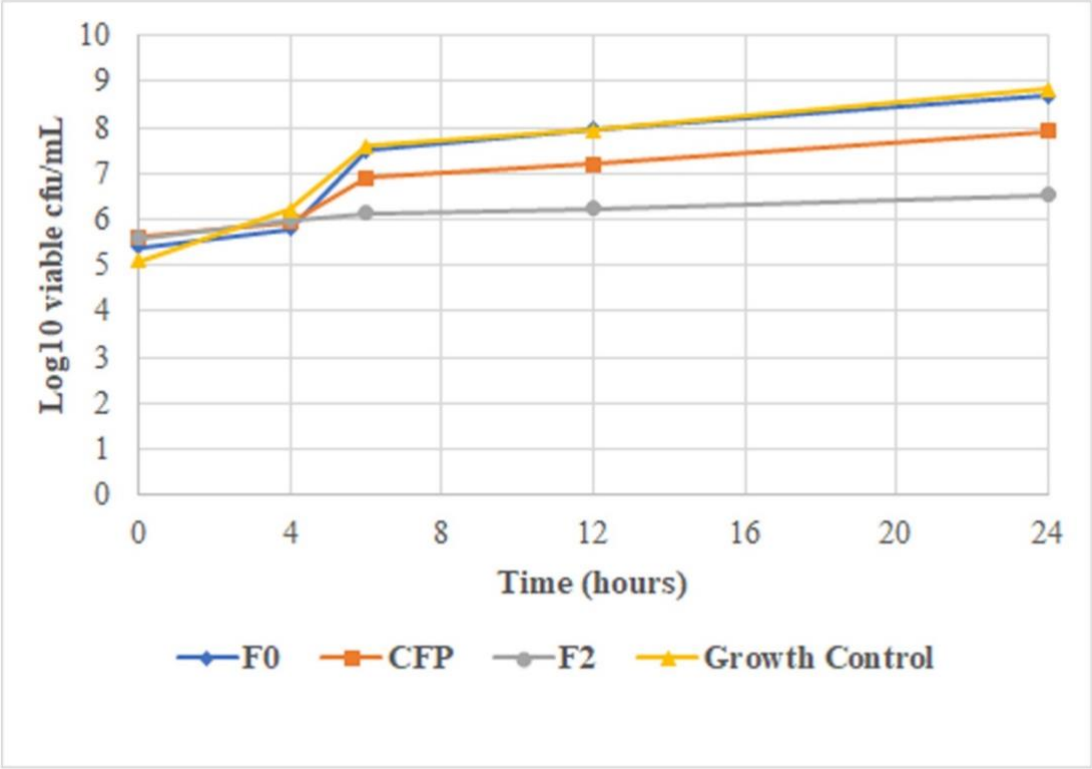

Figure 8: Time-kill results for *E.coli* ATCC 25922

2.10. Cytotoxicity profile

The cytotoxicity profiles of CFP, F0, and F2 were assessed in BEAS-2B and HepG2 cells in order to predict *in vitro* toxicity profiles of test materials in the main target organ, therapeutically in the lungs, and in the liver due to its metabolic capacity. MTT-based cytotoxicity profiles of tested samples in both acute (24 h) and long-term (72 h) exposure conditions, neither CFP, F0 nor F2 has shown significant cytotoxicity in both cells with relative cell viability above 70% compared to the control according to ISO standard in our study (Figure 9) [33]. Therefore, the IC_{50} (inhibiting concentration of 50%) values of tested samples were above the highest tested concentration in both BEAS-2B and HepG2 cells according to the 24 h exposure. In addition, exposure to F2 led to an increase in the cell proliferation rate in BEAS-2B bronchial epithelia dose-dependently. However, the long-term exposure to CFP, F0, and F2 affected the cell viability rates remarkably in both HepG2 and BEAS-2B cells. As depicted in Figure 9, the cell viabilities in BEAS-2B and HepG2 cells were higher with the exposure to F2 (200 µg/ml) compared to F0 (100 µg/ml) and CFP (100 µg/ml) alone.

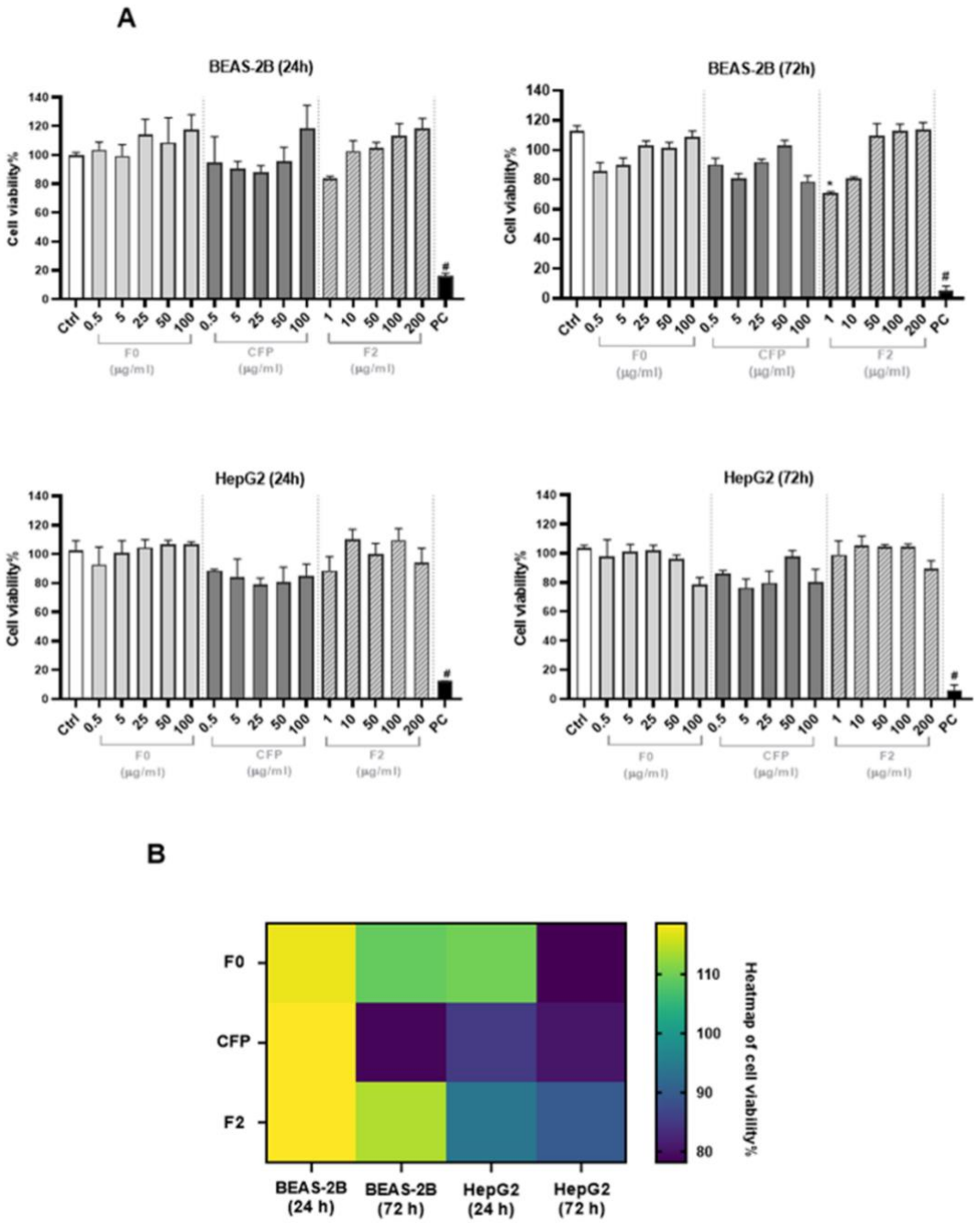

Figure 9: Cytotoxicity profile of F0, CFP and F2 in BEAS-2B and HepG2 cells for 24 and 72 h.

A: Relative cell viabilities in BEAS-2B and HepG2 cells for 24 and 72 h. Statistical differences between Ctrl vs. groups $^{*}p<0.05$; $^{\#}p<0.01$. **B:** Heatmap of relative cell viability of BEAS-2B and HepG2 cells exposed to the highest experimental doses. F0 and CFP: 100µg/ml; F2: 200µg/ml. CFP: Cefpodoxime proxetil; Ctrl: Control (DMSO 0.5%, v/v); PC (Positive control): DMSO (20%, v/v); F0: Blank nanoparticles; F2: Cefpodoxime nanoparticles 1:2 (drug: polymer).

3. DISCUSSION

The determination of the smallest particle size in the blank nanoparticle can be associated with the fact that it is not loaded with drugs. In a study by Koopaei et al., Roxithromycin-loaded PEG-PLGA nanoparticles were developed and it was observed that the particle size increased as the encapsulation efficiency of the nanoparticles increased [22]. The larger particle size of F2 compared to F1 may be related to the higher polymer: drug ratio used during preparation in F2. Similarly, in a study by Hasan et al., levofloxacin-loaded eudragit nanoparticles were prepared and an increase in particle size was observed by changing the drug: polymer ratio from 1:1 to 1:2 [34]. Polydispersity describes the degree of non-uniformity in the size distribution

of particles. PDI is used to define the size range of nanocarriers. >0.7 PDI values indicate a very broad particle size distribution of particles [35]. It could be said that blank and CFP nanoparticles showed uniform particle size distribution. Particles with low particle size distribution make the formulation more stable by slowing the Ostwald ripening [36]. Zeta potential can be defined as the potential difference between the dispersion medium and dispersed particles. It affects the physicochemical characteristics and cellular uptake of nanocarriers [37]. 20-40 mV zeta potential value indicates the physical stability of the nanocarrier and less prone to form aggregates [38]. In this case, it can be said that the zeta potential values of drug-loaded nanoparticles are compatible with the criteria. The positive charge of nanoparticles can be associated with the cationic structure of ERS. The reason for the difference in encapsulation efficiency can be explained by the different polymer ratios. The higher entrapment efficiency in F2 may be due to the higher polymer: drug ratio. Similarly in the study of Jelvehgari et al., it was observed that the production yield increased by increasing the cellulose acetate phthalate: mefenamic acid ratio from 0.75:1 to 1.25:1 [39]. Subsequent experiments were carried out with F2 which was chosen as the main formulation because it had a higher EE%, suitable size, zeta potential, and PDI.

SEM images clearly indicate that nanoparticles have a monodisperse distribution in shape compared to CFP. In addition, a reduction in the particle size of CFP was demonstrated during the nanoparticle manufacturing process. A similar reduction in the size of the pure drug during the formulation process was reported in the Efavirenz-loaded Eudragit-E100 nanoparticles developed by Hari and co-workers [40].

Similar peaks were observed in the F0 and F2 thermograms between 0-200°C. In the literature, a similar DSC pattern was observed between the cefpodoxime-loaded nanoparticles and blank nanoparticles supporting this data [41]. The sharp endothermic peak of CFP at 96°C was not observed in the thermogram of F2 due to the decrease in the crystallinity of the drug after encapsulation in the polymer. In addition, any new peak belonging to CFP was not detected in the DSC thermogram of F2, indicating that CFP was uniformly dispersed in nanoparticles. This is evidence that there is no undesirable interference and incompatibility between the drug and the polymer [42].

All of the samples showed diffused peaks due to their amorphous nature. In addition, the absence of a CFP peak in the XRD pattern of F2 indicates that the drug has been successfully entrapped in the nanoparticle. Similarly in the literature, the characteristic peak of vildagliptin in the XRD pattern disappeared in the XRD pattern of vildagliptin-loaded ERS microspheres [43].

The FT-IR spectra of F0 and ERS are similar in terms of the localization and intensity of peaks. In the spectra of F2, characteristic peaks of CFP (1271 and 1531 cm^{-1}) were not observed due to the encapsulation of the drug into the polymeric nanoparticle. Also, the spectrum of F0 and F2 showed no interactions between the drug and polymer. Similarly, in the study of Park et al., PLGA nanoparticles loaded with Bovine Serum Albumin (BSA) were developed, and in FT-IR studies, it was observed that the main signals of BSA were lost in the spectrum of the drug-loaded nanoparticles [44].

The fact that both polymer and CFP peaks were observed in the ^{1}H-NMR spectrum of F2 confirms the molecular distribution of CFP in the polymeric matrix. In addition, the absence of an additional CFP signal indicates that there is no direct chemical bonding between the polymer and the drug [45]. When the ^{1}H-NMR spectra of CFP and F2 were compared, it was observed that the intensity of the peaks corresponding to CFP is less in nanoparticles. This may be attributed to the fact that CFP is entrapped in the polymeric matrix and the amount of CFP exposed to the solvent is less [46].

When the drug release rates of nanoparticle formulations are examined, it can be said that there is a burst effect in F1. This can be explained by the adhesion of drug molecules to the nanoparticle surface during the preparation of the nanoparticle formulation [47]. The F2 formulation showed a controlled release profile in contrast to F1 and free CFP, which is advantageous in providing a better therapeutic potential by overcoming the side effects associated with long-term use of the drug [48].

According to the 2-hour release profile of CFP and nanoparticles, CFP showed a higher rate of release in the gastric environment than in the intestinal environment. This may be associated with greater dissolution of CFP in an acidic medium [49]. When the release profile of nanoparticles was examined, both F1 and F2 showed higher cumulative drug release in a pH 7.4 environment. This can be explained by the fact that the ERS polymer, in which the drug is entrapped, shows higher solubility above pH 7 and thus releases the drug at a higher rate [50].

Drug release profiles were evaluated in terms of kinetic models. Korsmeyer-Peppas indicates the controlled release of a drug molecule from a polymeric matrix by swelling which is compatible with the drug release profile of F1 and F2 [32]. According to the kinetic results of F1 and F2, it could be stated that the controlled-release polymeric matrix systems were prepared.

According to EUCAST, both CFP and F2 were detected in the sensitive range for *E.coli*. In the study conducted by Yurtdaş-Kırımlıoğlu and Görgülü, the effectiveness of CFP nanoparticles developed with ERS100 on *E.coli* and *Staphylococcus aureus* was investigated. In their study, it was reported that CFP entrapped with ERS100 showed a lower MIC value than pure CFP. It is observed that the study conducted by Yurtdaş-Kırımlıoğlu and Görgülü gave results in parallel with our study [51]. The antimicrobial activity of self-nanoemulsifying drug delivery system (SNEDDS) on *Staphylococcus aureus* ATCC 25922, *Escherichia coli* ATCC 29213, *Bacillus subtilis* ATCC was investigated by Bajaj et al. When the data obtained with *E.coli* were examined, it was observed that a MIC result of approximately 1.5 µg/mL was achieved for both pure CFP and CFP-SNEDDS [52].

The time-kill results obtained from the formulations are discussed. No other study investigating the time-kill activity of cefpodoxime has been found in the literature. In this context, our study is the first to examine the time-kill activity of cefpodoxime. Ceftriaxone, a third-generation cephalosporin drug-like cefpodoxime, was studied by Mushtaq et al. Their study examined the activity of ceftriaxone-loaded chitosan nanoparticles (CNPs) on clinical Methicillin resistance *S.aureus* and *E.coli* isolates. In terms of cell viability, similarly, ceftriaxone-loaded CNPs reduced *E.coli* viability at the end of 24 hours in the study of Mushtaq and colleagues [53]. In light of all experimental results evaluated, it was revealed that F2 was more effective and stable than CFP in the 24-hours. F2 showed a controlled drug release and prolonged antibacterial activity.

There are limited studies on the *in vitro* cytotoxicity profile of cefpodoxime alone or loaded as nanoparticles. The only study performed previously by Yurtdaş-Kırımlıoğlu and Görgülü revealed that CFP exhibited dose and time-dependent cytotoxicity in CCD-19Lu human pulmonary epithelial cells up to 50 µg/ml for 2, 48, and 72 h [51]. In the present study, we evaluated the *in vitro* cytotoxicity profile of CFP (0.5-100 µg/ml) and F2 (1-200 µg/ml) first time in both therapeutic target bronchial epithelial and liver epithelial since it is involved in the metabolic pathway of CFP.

4. CONCLUSION

CFP-loaded nanoparticles were evaluated for the first time based on their ability to time-kill potency, *in vitro* therapeutic target, and metabolism organ cytotoxicity. Our findings revealed that these nanoparticles exhibited a controlled release profile with long-term antibacterial activity. Thus, the ideally selected F2 formulation stopped *E.coli* growth for 24 hours. This development is highly promising as it indicates the potential to decrease the frequency of the drug dosage. Moreover, CFP-loaded nanoparticles were found to be non-cytotoxic in acute and long-term exposure conditions in human bronchial and liver epithelial cells. Therefore, promising results were obtained in terms of safety as well as the superior success of the F2 formulation in antibacterial efficacy. In light of the results obtained, it can be said that CFP-loaded nanoparticles have suitable physicochemical and drug-delivery system properties. It has been shown by microbiological and cytocompatibility studies that it is suitable for use in the treatment of bacterial infections. Hence, the use of CFP-loaded ERS nanoparticles against bacterial infections can be a promising drug delivery system in the treatment, as it is predicted to provide a long-term antibacterial effect and show fewer side effects.

5. MATERIALS AND METHODS

5.1. Materials

Cefpodoxime proxetil was a kind gift of Ali Raif İlaç Sanayi A.Ş (Istanbul/Turkey). ERS was kindly donated by Evonik Industries (Istanbul/Turkey). Poly(vinyl alcohol) (PVA, MW=30000-70000), acetone, and methanol were purchased from Sigma-Aldrich (Germany). ortho-Phosphoric acid 85% was purchased from Merck (Germany). Mueller-Hinton Agar (MHA), Mueller-Hinton broth (MHB), and Tryptic Soy Agar (TSA) were purchased from Merck (Germany) and used in antibacterial activity, and time-kill assay. Dulbecco's Modified Eagle's Medium (DMEM), fetal bovine serum (FBS), and antibiotics (10.000 µg/mL streptomycin and 10.000 units/mL penicillin) used in the cell culture studies were all from Gibco (USA) and molecular biology grade dimethyl sulfoxide (DMSO), 3-(4,5-Dimethylthiazol-2-yl)-2,5-Diphenyltetrazolium bromide (MTT), and isopropanol was purchased from Sigma-Aldrich (Germany). All other chemicals used were of analytical grade.

5.2. Preparation of CFP-loaded ERS nanoparticles

Blank nanoparticles (F0) and CFP-loaded nanoparticles (F1 and F2) were prepared by a single emulsion solvent evaporation method [54,55]. CFP and ERS were dissolved in acetone at room temperature under a

magnetic stirrer. This organic phase was slowly injected (0.5 mL/min) into the aqueous phase containing 20 mL, 1% PVA (w/v%) with continuous stirring at 600 rpm. After the injection, the oil/water emulsion was sonicated with 70% amplitude for 5 minutes under a probe sonicator. The resulting nanoparticle suspension was stirred overnight at room temperature to evaporate the organic solvent. Nanoparticles were then collected by ultracentrifuge of the mixture at 13500 rpm for 20 minutes at room temperature. Collected nanoparticles were washed three times with ultrapure water and centrifuged to remove the adsorbed drug and solvent residue. Nanoparticles were redispersed with ultrapure water and lyophilized by a freeze dryer for 48 hours. Obtained nanoparticles were stored at -20°C for further experiments. Blank nanoparticles were prepared using the same procedure without adding CFP. The components of each formulation were summarized in Table 1.

5.3. Particle size, polydispersity index (PDI), and zeta potential measurement

The particle size distribution and PDI of nanoparticles were determined by Photon Correlation Spectroscopy (PCS) at a 90° scattering angle and 25°C temperature using Malvern Nano-ZS (Malvern Instruments, United Kingdom). Zeta potential was measured using a disposable zeta cuvette by the same instrument. Each sample was measured in triplicate and mean±standard deviation values were reported.

5.4. Quantification of CFP by high-performance liquid chromatography (HPLC)

The entrapment efficiency (EE%) and *in vitro* release of samples were quantified by HPLC (Shimadzu, Japan) using a method validated for precision, accuracy, and linearity [56]. CFP was analyzed using ACE-5 column (C_{18} 46x250 mm, 5 µm). The mobile phase was prepared by mixing methanol:water (70:30, v/v), and pH was maintained at 3 using 85% ortho-phosphoric acid and pumped at an isocratic flow rate of 1 mL/min. A constant amount of 20 µL samples were injected via an automatic injector and the wavelength was set to 240 nm for determination with a photodiode array (PDA) detector. The column oven was adjusted to 25°C. A stock solution of CFP was prepared in methanol with 1000 µg/mL concentration and the linearity was studied with samples in the concentration range of 10-250 µg/mL prepared by diluting the stock solution with the mobile phase.

5.5. Determination of entrapment efficiency (EE%)

For the determination of EE% in F1 and F2, 10 mg samples were fully dissolved in 5 mL dimethyl sulfoxide (DMSO) under sonication separately. The obtained clear samples were mixed with a vortex and filtered through a 0.2 µm membrane filter. The filtrates were diluted 10 times with the mobile phase and analyzed by the HPLC method previously described. EE% of nanoparticles was calculated according to Equation 1. The experiments were carried out in triplicate and mean±standard deviation values were reported.

$$EE\% = 100x\frac{amount\ of\ CFP\ incorporated\ in\ nanoparticles}{amount\ of\ CFP\ used\ in\ preparation\ of\ nanoparticles} \qquad \text{(Equation 1)}$$

5.6. Morphological analysis of nanoparticles

The shape and surface morphology of CFP and nanoparticles were determined using a Scanning Electron Microscope (SEM) by FEI Quanta FEG 650 SEM (Hillsboro, OR, USA). Samples were coated with gold and analysis was performed under a high vacuum.

5.7. Differential scanning calorimetry (DSC) analysis

The physical state and crystallinity properties of CFP nanoparticles were investigated using differential scanning calorimetry (DSC) by DSC-60 (Shimadzu, Japan) between 30-500°C. The accurately weighed samples (5±0,1 mg) were located in aluminum pans and sealed hermetically. The analysis was performed under nitrogen gas with a flow rate of 50 mL/min and a heating rate of 10°C/min.

5.8. X-ray diffraction (XRD) analysis

The XRD patterns of CFP, blank nanoparticles, and CFP nanoparticles were recorded using PANalytical EMPYREAN XRD (Almelo, The Netherlands) in order to determine the crystallinity of the drug. The samples were analyzed using a 2θ angle in the range of 2-40° with a 2°/min scanning rate.

5.9. Fourier transform infrared (FT-IR) spectroscopy

FT-IR spectra for CFP, ERS, blank nanoparticles, and CFP nanoparticles were revealed by means of an FT-IR-8300 spectrophotometer (Shimadzu, Japan) within the wavelength range of 4000-400 cm^{-1}. Analysis was carried out directly with the solid sample.

5.10. Proton nuclear magnetic resonance (^{1}H-NMR) spectroscopy

^{1}H-NMR analyses were conducted using Varian Mercury-plus AS-400 NMR (Agilent, USA). Blank nanoparticles and CFP nanoparticles were tested using deuterated DMSO (DMSO-D6) as the solvent.

5.11. *In vitro* drug release profile and release kinetics

In vitro release pattern of CFP and nanoparticles was studied over 24 hours using a dialysis method [57]. 2 mg CFP and nanoparticles carrying an equivalent amount of CFP were placed in a cellulose acetate dialysis bag (molecular weight cut-off 12-14 kDa, Sigma Aldrich, USA) with 1 mL distilled water separately and locked by special clamps. The dialysis bag was then immersed into a beaker consisting of 100 mL, 0.1 N HCl buffer (pH 1.2) with a continuous stirring rate of 100 rpm at 37±0,5°C. After 2 hours, the HCl buffer was replaced with the same volume of phosphate buffer saline (pH 7.4) for 22 hours. Samples were withdrawn in dissolution medium and the same amount of fresh medium was replaced periodically. After this procedure, the beaker was covered with parafilm in order to prevent evaporation of the dissolution medium. The withdrawn samples were analyzed by the validated HPLC method previously described. Sink condition was ensured. The experiments were run in triplicate. Results were evaluated as mean±standard deviation and an *in vitro* release graph was drawn using cumulative release percentage values against time. The *in vitro* release studies were fitted to mathematical modeling which defines the data about the release behavior of formulation. The release kinetics were evaluated by the DDSolver add-in program on Microsoft Excel [29].

5.12. Antibacterial activity test

Escherichia coli ATCC 25922 was used to evaluate the antibacterial activity of CFP and nanoparticles. Inhibitory activities of the formulations and CFP were investigated by the broth microdilution method [58]. Minimum inhibitory concentrations (MICs) values of CFP and nanoparticles were determined in accordance with the European Committee on Antimicrobial Susceptibility Testing (EUCAST) criteria. The bacterial strain was grown on Mueller-Hinton Agar (MHA) (Merck, Germany), at 37 °C for 24 h. Fresh colonies of *E.coli ATCC 25922* were suspended in physiological saline. Bacterial suspension, which was adjusted to 0.5 McFarland standard, was diluted 100 times in Mueller-Hinton broth (MHB) (Merck, Germany). Serial dilutions of the formulations were performed using sterile 96-well microdilution plates with MHB to set the concentrations from 2048 µg/ml to 1 µg/ml. Plates were incubated at 37°C for 24 hours after adding to each well bacterial inoculum. Growth control and sterility control were also tested. The lowest concentration that inhibits microbial growth is defined as MIC. Experiments were done in triplicate (n=3).

5.13. Time-kill assay

In terms of pharmacodynamics, the time-kill assay allows the study of concentration-dependent and time-dependent bactericidal activities of antimicrobial agents. The time-kill activity of CFP and nanoparticles was studied in this research. MIC values acquired via broth microdilution procedure were utilized in the time-kill assay. Formulations were diluted into an MHB medium to establish MIC and sub-MIC concentrations. Bacterial suspensions were fixed to 10^5 CFU/mL. The control tube (without formulation) and tubes containing the formulation were inoculated with bacterial suspensions. All of them were incubated in a shaker incubator at 200 rpm, 37°C. 50 µL aliquots of overnight culture were taken and diluted with saline, then inoculated into Tryptic Soy Agar (TSA) (Merck, Germany) at time intervals (0, 4th, 6th, 12th, and 24th hours). The inoculated TSA plates were incubated at 37°C, for 24 hours. After incubation, the bacterial colonies on agar plates were determined by the plate counting method. The number of bacterial colonies was calculated as CFU/mL [59]. The procedure was performed in triplicate (n=3). The curve of log CFU/ml was plotted against time. Experiments were carried out in triplicate (n=3).

5.14. Cytotoxicity assay

For predictive analysis of main target organ toxicity, BEAS-2B human bronchial epithelial cell (CRL-9609™) and HepG2 human liver adenocarcinoma (HB-8065™) cell lines (ATCC, USA) were cultured in DMEM (5% FBS, v/v) and DMEM (10% FBS, v/v), respectively and supplemented with 1% antibiotics at 37°C in a humidified atmosphere of 5% CO_2. For the assessment of the cytotoxicity profile of CFP, ERS, and CFP

nanoparticles, the BEAS-2B and HepG2 cells were plated in 96-well microplates as $2x10^5$ cell/mL for 24 h exposure and as $0.5x10^5$ cell/mL for a 72 h exposure and incubated at 37°C in 5% CO_2. On the following day of seeding, the cells were treated with CFP and F0 between 0.5-100 µg/mL dissolved in DMSO, whereas F2 was applied between 1-200 µg/mL to compare the similar amounts of active ingredient applied via CFP-loaded ERS nanoparticles exposure. At the end of each incubation, the culture mediums were discarded and 0.5 mg/mL MTT was added to each well for an additional 2 h at 37°C. After 2 h incubation, the medium was discarded and 100 µL of isopropanol (Sigma Aldrich, USA) was added to wells to dissolve formazan crystals. The optical density was measured at 570 nm wavelengths using a microplate reader (Thermo Varioskan, Singapore). The percentage of cell viability was detected as briefly described in our previous study [60]. According to the test protocol (ISO, 2009), a reduction of cell viability by more than 30% is considered a cytotoxic effect compared to the control group.

5.15. Statistical analysis

Each experiment was carried out three independent times and the data are presented as mean±standard deviation (SD). The statistical significance of the differences in particle size, zeta potential values, PDI, and EE% between the nanoparticle formulations were tested by one-way analysis of variance (ANOVA). Microsoft Excel and DDSolver add-in program was employed for the *in vitro* release kinetics calculations. The statistical significance of cytotoxicity data was evaluated by GraphPad Prism (8.0) (La Jolla, California, US) via one-way ANOVA. Differences between the evaluated values were considered statistically significant at a level of $p \leq 0.05$.

Acknowledgements: The authors would like to thank Prof. Dr. Serdar Ünlü and Ali Raif İlaç Sanayi A.Ş (Istanbul/Turkey) for their kind gift of Azithromycin dihydrate and Evonik Industries (Istanbul/Turkey) for the kind gift of Eudragit RS 100. In addition, the authors are appreciated to ARGEFAR-Center for Drug Research and Development and Pharmacokinetic Applications, Ege University for device support in the analyses.

Author contributions: Concept – I.A.; Design – I.A.; Supervision –I.A.; Resources – I.A., A.A., R.R.; Materials – I.A., A.A., R.R.; Data Collection and/or Processing – I.A., A.A., R.R.; Analysis and/or Interpretation – I.A., A.A., R.R.; Literature Search – I.A., A.A., R.R.; Writing – I.A., A.A., R.R.; Critical Reviews – I.A., A.A., R.R.

Conflict of interest statement: The authors declared no conflict of interest.

REFERENCES

[1] Pridgen EM, Alexis F, Farokhzad OC. Polymeric nanoparticle drug delivery technologies for oral delivery applications. Expert Opin Drug Deliv. 2015; 12(9): 1459–73. https://doi.org/10.1517/17425247.2015.1018175

[2] Banerjee A, Qi J, Gogoi R, Wong J, Mitragotri S. Role of nanoparticle size, shape and surface chemistry in oral drug delivery. J Control Release. 2016; 238: 176–85. https://doi.org/10.1016/J.JCONREL.2016.07.051

[3] Madkour LH. Nanoparticle and polymeric nanoparticle-based targeted drug delivery systems. Nucleic Acids as Gene Anticancer Drug Deliv Ther. 2019; 191–240. https://doi.org/10.1016/B978-0-12-819777-6.00013-5

[4] Li Y, Gao GH, Lee DS. Stimulus-Sensitive Polymeric Nanoparticles and Their Applications as Drug and Gene Carriers. Adv Healthc Mater. 2013; 2(3): 388–417. https://doi.org/10.1002/ADHM.201200313

[5] Trapani A, Laquintana V, Denora N, Lopedota A, Cutrignelli A, Franco M, Trapani G. Eudragit RS 100 microparticles containing 2-hydroxypropyl-β-cyclodextrin and glutathione: Physicochemical characterization, drug release and transport studies. Eur J Pharm Sci. 2007; 30(1): 64–74. https://doi.org/10.1016/J.EJPS.2006.10.003

[6] Jelvehgari M, Barar J, Valizadeh H, Shadrou S, Nokhodchi A. Formulation, characterization and in vitro evaluation of theophylline-loaded Eudragit RS 100 microspheres prepared by an emulsion-solvent diffusion/evaporation technique. Pharm Dev Technol. 2011; 16(6): 637–44. https://doi.org/10.3109/10837450.2010.508075

[7] Dehghani MA, Maram NS, Moghimipour E, Khorsandi L, Atefikhah M, Mahdavinia M. Protective effect of gallic acid and gallic acid-loaded Eudragit-RS 100 nanoparticles on cisplatin-induced mitochondrial dysfunction and inflammation in rat kidney. Biochim Biophys Acta - Mol Basis Dis. 2020; 1866(12). https://doi.org/10.1016/J.BBADIS.2020.165911

[8] Payab S, Jafari-Aghdam N, Barzegar-Jalali M, Mohammadi G, Lotfipour F, Gholikhani T, Adibkia K. Preparation and physicochemical characterization of the azithromycin-Eudragit RS 100 nanobeads and nanofibers using electrospinning method. J Drug Deliv Sci Technol. 2014; 24(6): 585–90. https://doi.org/10.1016/S1773-2247(14)50123-2

[9] Real DA, Gagliano A, Sonsini N, Wicky G, Orzan L, Leonardi D, Salomon C. Design and optimization of pH-sensitive

Eudragit nanoparticles for improved oral delivery of triclabendazole. Int J Pharm. 2022; 617: 121594. https://doi.org/10.1016/J.IJPHARM.2022.121594

[10] Valizadeh H, Mohammadi G, Ehyaei R, Milani M, Azhdarzadeh M, Zakeri-Milani P, Lotfipour F. Antibacterial activity of clarithromycin loaded PLGA nanoparticles. Pharmazie. 2012; 67(1): 63–8. https://doi.org/10.1691/ph.2012.1052

[11] Kumar V, Madabushi R, Lucchesi MBB, Derendorf H. Pharmacokinetics of cefpodoxime in plasma and subcutaneous fluid following oral administration of cefpodoxime proxetil in male beagle dogs. J Vet Pharmacol Ther. 2011; 34(2): 130–5. https://doi.org/10.1111/J.1365-2885.2010.01198.X

[12] Mostafa GAE, Al-Otaibi YH, Al-Badr AA. Cefpodoxime proxetil. In: Profiles of Drug Substances, Excipients and Related Methodology. Academic Press; 2019. p. 1–165. https://doi.org/10.1016/bs.podrm.2019.02.001

[13] Fulton B, Perry CM. Cefpodoxime proxetil: a review of its use in the management of bacterial infections in paediatric patients. Paediatr Drugs. 2001; 3(2): 137–58. https://doi.org/10.2165/00128072-200103020-00006

[14] Arafa MG, Mousa HA, Afifi NN. Preparation of PLGA-chitosan based nanocarriers for enhancing antibacterial effect of ciprofloxacin in root canal infection. Drug Deliv. 2020; 27(1): 26. https://doi.org/10.1080/10717544.2019.1701140

[15] Zielinska A, Carreiró F, Oliveira AM, Neves A, Pires B, Venkatesh DN, Durazzo A, Lucarini M, Eder P, Silva AM, Santini A, Souto EB. Polymeric Nanoparticles: Production, Characterization, Toxicology and Ecotoxicology. Mol 2020, Vol 25, Page 3731. 2020; 25(16): 3731. https://doi.org/10.3390/MOLECULES25163731

[16] Sánchez A, Mejía SP, Orozco J. Recent Advances in Polymeric Nanoparticle-Encapsulated Drugs against Intracellular Infections. Molecules. 2020; 25(16). https://doi.org/10.3390/MOLECULES25163760

[17] Kadian R. NANOPARTICLES: A PROMISING DRUG DELIVERY APPROACH. Asian J Pharm Clin Res. 2018; 11(1): 30–5. https://doi.org/10.22159/AJPCR.2018.V11I1.22035

[18] Jindal AB. The effect of particle shape on cellular interaction and drug delivery applications of micro- and nanoparticles. Int J Pharm. 2017; 532(1): 450–65. https://doi.org/10.1016/J.IJPHARM.2017.09.028

[19] Prabha S, Arya G, Chandra R, Ahmed B, Nimesh S. Effect of size on biological properties of nanoparticles employed in gene delivery. Artif Cells, Nanomedicine Biotechnol. 2016; 44(1): 83–91. https://doi.org/10.3109/21691401.2014.913054

[20] Chen X, Wang T, Lu M, Zhu L, Wang Y, Zhou WZ. Preparation and evaluation of tilmicosin-loaded hydrogenated castor oil nanoparticle suspensions of different particle sizes. Int J Nanomedicine. 2014; 9(1): 2655–64. https://doi.org/10.2147/IJN.S58898

[21] Vladár AE, Hodoroaba VD. Characterization of nanoparticles by scanning electron microscopy. Charact Nanoparticles Meas Process Nanoparticles. 2020; 7–27. https://doi.org/10.1016/B978-0-12-814182-3.00002-X

[22] Koopaei MN, Maghazei MS, Mostafavi SH, Jamalifar H, Samadi N, Amini M, Malek SJ, Darvishi B, Atyabi F, Dinarvand R. Enhanced antibacterial activity of roxithromycin loaded pegylated poly lactide-co-glycolide nanoparticles. DARU, J Pharm Sci. 2012; 20(1). https://doi.org/10.1186/2008-2231-20-92

[23] Singh I, Rana V. Exploiting the interaction of polymethacrylates with iron oxide for the enhancement of mucoadhesive strength. Pak J Pharm Sci. 2014; 27(2): 343–50.

[24] Türk CT, Hasçiçek C, Gönül N. Evaluation of drug-polymer interaction in polymeric microspheres containing diltiazem hydrochloride. J Therm Anal Calorim. 2009; 95(3): 865–9. https://doi.org/10.1007/S10973-007-8605-7

[25] Sukhbir S, Yashpal S, Sandeep A. Development and statistical optimization of nefopam hydrochloride loaded nanospheres for neuropathic pain using Box–Behnken design. Saudi Pharm J. 2016; 24(5): 588–99. https://doi.org/10.1016/j.jsps.2015.03.020

[26] Shim JB, Kim MJ, Kim SJ, Kang SJ, Lee JH, Kim HS, Lee D, Khang G. Dissolution properties of control released solid dispersion of carvedilol with HPMC and Eudragit RS. J Pharm Investig. 2012; 42(5): 285–91. https://doi.org/10.1007/S40005-012-0037-0

[27] Ben ES, Nofita R, Rusdi S, Suardi M, Djamaan A. Use of eudragit RS PO in the formulation of acyclovir hollow-microspheres by solvent evaporation technique. Der Pharm Lett. 2016; 8(11): 53–9.

[28] Pilaniya K, Chandrawanshi HK, Pilaniya U, Manchandani P, Jain P, Singh N. Recent trends in the impurity profile of pharmaceuticals. J Adv Pharm Technol Res. 2010; 1(3): 302–10. https://doi.org/10.4103/0110-5558.72422

[29] Zhang Y, Huo M, Zhou J, Zou A, Li W, Yao C, Xie S. DDSolver: An Add-In Program for Modeling and Comparison of Drug Dissolution Profiles. AAPS J. 2010; 12(3): 263. https://doi.org/10.1208/S12248-010-9185-1

[30] Costa P, Lobo JMS. Modeling and comparison of dissolution profiles. Eur J Pharm Sci. 2001; 13(2): 123–33.

https://doi.org/10.1016/S0928-0987(01)00095-1

[31] Kulpreechanan N, Sorasitthiyanukarn FN. Evaluation of in vitro release kinetics of capsaicin-loaded chitosan nanoparticles using DDsolver. Int J Res Pharm Sci. 2020; 11(3): 4555–9. https://doi.org/10.4028/www.scientific.net/MSF.998.277

[32] Marcos Luciano Bruschi. Strategies to Modify the Drug Release from Pharmaceutical Systems [homepage on the Internet]. Strategies to Modify the Drug Release from Pharmaceutical Systems. 2015 [cited 2022 May 5].

[33] International Organization for Standardization. Biological Evaluation of Medical Devices Part 5: Tests for in vitro cytotoxicity (ISO 10993-5:2009). Biomed Saf Stand. 1996; 26(7): 54.

[34] Hasan AA, Sabry SA, Abdallah MH, El-damasy DA. Formulation and in vitro characterization of poly(dl-lactide-co-glycolide)/Eudragit RLPO or RS30D nanoparticles as an oral carrier of levofloxacin hemihydrate. Pharm Dev Technol. 2016; 21(6): 655–63. https://doi.org/10.3109/10837450.2015.1041044

[35] Danaei M, Dehghankhold M, Ataei S, Davarani HF, Javanmard R, Dokhani A, Khorasani S, Mozafari MR. Impact of particle size and polydispersity index on the clinical applications of lipidic nanocarrier systems. Pharmaceutics. 2018; 10(2). https://doi.org/10.3390/pharmaceutics10020057

[36] Aghajani M, Shahverdi AR, Amani A. The use of artificial neural networks for optimizing polydispersity index (PDI) in nanoprecipitation process of acetaminophen in microfluidic devices. AAPS PharmSciTech. 2012; 13(4): 1293–301. https://doi.org/10.1208/S12249-012-9859-3

[37] Honary S, Zahir F. Effect of zeta potential on the properties of nano-drug delivery systems - A review (Part 1). Trop J Pharm Res. 2013; 12(2): 255–64. https://doi.org/10.4314/TJPR.V12I2.19

[38] Samimi S, Maghsoudnia N, Eftekhari RB, Dorkoosh F. Lipid-Based Nanoparticles for Drug Delivery Systems. Charact Biol Nanomater Drug Deliv Nanosci Nanotechnol Drug Deliv. 2019; 47–76. https://doi.org/10.1016/B978-0-12-814031-4.00003-9

[39] Jelvehgari M, Hassanzadeh D, Kiafar F, Loveymi BD, Amiri S. Preparation and Determination of Drug-Polymer Interaction and In-vitro Release of Mefenamic Acid Microspheres Made of CelluloseAcetate Phthalate and/or Ethylcellulose Polymers. Iran J Pharm Res IJPR. 2011; 10(3): 457.

[40] Hari BNV, Narayanan N, Dhevendaran K, Ramyadevi D. Engineered nanoparticles of Efavirenz using methacrylate co-polymer (Eudragit-E100) and its biological effects in-vivo. Mater Sci Eng C. 2016; 67: 522–32. https://doi.org/10.1016/j.msec.2016.05.064

[41] Mujtaba A, Ali M, Kohli K. Formulation of extended release cefpodoxime proxetil chitosan-alginate beads using quality by design approach. Int J Biol Macromol. 2014; 69: 420–9. https://doi.org/10.1016/j.ijbiomac.2014.05.066

[42] Sharma M, Gupta N, Gupta S. Implications of designing clarithromycin loaded solid lipid nanoparticles on their pharmacokinetics, antibacterial activity and safety. RSC Adv. 2016; 6(80): 76621–31. https://doi.org/10.1039/C6RA12841F

[43] Naik JB, Waghulde MR. Development of vildagliptin loaded Eudragit® microspheres by screening design: in vitro evaluation. J Pharm Investig. 2018; 48(6): 627–37. https://doi.org/10.1007/s40005-017-0355-3

[44] Park MH, Baek JS, Lee CA, Kim DC, Cho CW. The effect of Eudragit type on BSA-loaded PLGA nanoparticles. J Pharm Investig. 2014; 44(5): 339–49. https://doi.org/10.1007/s40005-014-0129-0

[45] Simeonova M, Rangel M, Ivanova G. NMR study of the supramolecular structure of dual drug-loaded poly(butylcyanoacrylate) nanoparticles. Phys Chem Chem Phys. 2013; 15(39): 16657–64. https://doi.org/10.1039/C3CP51471D

[46] Sarika PR, James NR, Anilkumar PR, Raj DK. Preparation, characterization and biological evaluation of curcumin loaded alginate aldehyde–gelatin nanogels. Mater Sci Eng C. 2016; 68: 251–7. https://doi.org/10.1016/J.MSEC.2016.05.046

[47] Almoustafa HA, Alshawsh MA, Chik Z. Technical aspects of preparing PEG-PLGA nanoparticles as carrier for chemotherapeutic agents by nanoprecipitation method. Int J Pharm. 2017; 533(1): 275–84. https://doi.org/10.1016/J.IJPHARM.2017.09.054

[48] Kalaydina RV, Bajwa K, Qorri B, Decarlo A, Szewczuk MR. Recent advances in "smart" delivery systems for extended drug release in cancer therapy. Int J Nanomedicine. 2018; 13: 4727–45. https://doi.org/10.2147/IJN.S168053

[49] Jabeen S, Hassan F, Yousuf RI, Shoaib MH, Israr F, Hasan SMF, Saeed R, Farooqi S. Impact of different organic acids on solubility enhancement of cefpodxime proxetil immediate release tablet and its stability studies. Pak J Pharm Sci. 2017; 30(3): 855–66.

[50] Franco P, de Marco I. Eudragit: A Novel Carrier for Controlled Drug Delivery in Supercritical Antisolvent Coprecipitation. Polym 2020, Vol 12, Page 234. 2020; 12(1): 234. https://doi.org/10.3390/POLYM12010234

[51] Yurtdaş-Kırımlıoğlu G, Görgülü Ş. Surface modification of PLGA nanoparticles with chitosan or Eudragit® RS 100: Characterization, prolonged release, cytotoxicity, and enhanced antimicrobial activity. J Drug Deliv Sci Technol. 2021; 61. https://doi.org/10.1016/J.JDDST.2020.102145

[52] Bajaj A, Rao MRP, Khole I, Munjapara G. Self-nanoemulsifying drug delivery system of cefpodoxime proxetil containing tocopherol polyethylene glycol succinate. Drug Dev Ind Pharm. 2013; 39(5): 635–45. https://doi.org/10.3109/03639045.2012.683440

[53] Mushtaq S, Khan JA, Rabbani F, Latif U, Arfan M, Yameen MA. Biocompatible biodegradable polymeric antibacterial nanoparticles for enhancing the effects of a third-generation cephalosporin against resistant bacteria. J Med Microbiol. 2017; 66(3): 318–27. https://doi.org/10.1099/JMM.0.000445

[54] Rao JP, Geckeler KE. Polymer nanoparticles: Preparation techniques and size-control parameters. Prog Polym Sci. 2011; 36(7): 887–913. https://doi.org/10.1016/J.PROGPOLYMSCI.2011.01.001

[55] Akartas I, Ates A. Desıgn of azıthromycın loaded eudragıt rl 100 nanopartıcles wıth extended antıbacterıal effect. Farmacia. 2023; 71(2): 345–58. https://doi.org/10.31925/FARMACIA.2023.2.15

[56] Hassan S, Iqbal S, Zaheer E, Hassan A, Hamid S, Ali M, Akram A, Maroof SZ, Abedin S, Khan SJ. Development and validation of RP-HPLC method for simultaneous determination of cefpodoxime proxetil and H2 receptor antagonists in pharmaceutical dosage forms. Pak J Pharm Sci. 2019; 32(2): 839–44.

[57] Akartas I, Karasulu HY. Preparation and characterization of self-microemulsifying drug delivery system (SMEDDS) of cisplatin for oral use in ovarian cancer treatment. Acta Pol Pharm - Drug Res. 2020; 77(1): 183–93. https://doi.org/10.32383/APPDR/114329

[58] EUCAST. European Committee on Antimicrobial Susceptibility Testing - Routine and extended internal quality control for MIC determination and disk diffusion as recommended by EUCAST. Version 120. 2022; 1–23.

[59] Balouiri M, Sadiki M, Ibnsouda SK. Methods for in vitro evaluating antimicrobial activity: A review. Vol. 6, Journal of Pharmaceutical Analysis. Elsevier; 2016. p. 71–9. https://doi.org/10.1016/j.jpha.2015.11.005

[60] Reis R, Orak D, Yilmaz D, Cimen H, Sipahi H. Modulation of cigarette smoke extract-induced human bronchial epithelial damage by eucalyptol and curcumin. Hum Exp Toxicol. 2021; 40(9): 1445–62. https://doi.org/10.1177/0960327121997986